Supplementary Material
for "Emergence of Broken Symmetry Via Odd Viscosity in Inertial Spinner Swarms"

CONTENTS

I. EXPERIMENT SETUP

The spinners consist of toothed acrylic discs which are laser-cut to have 24 teeth. The spinners were driven by 2 oppositely directed blowers (SUNON UB3-500B), driven at 3.7 volts by a LiIon 400 mA-hr battery (Adafruit 3898). The battery was sandwiched between 2 of the toothed discs, so that change in handedness of the spin could be accomplished by simple inversion of the disk. To ensure the consistency of the rotational driving torque, we made sure the batteries did not run more than 30 minutes after being charged to full.

A 60mm-diameter plastic Petri dish (Falcon Plastics) was used to lift the tooth wheel so that the close to elastic collisions with the taut wire of the air-table did not involve the teeth and hence little spin angular momentum change. An iPhone camera running at 30 frames/sec was used to take continuous movies of the dynamics of the spinner active matter. A bar-code imprinted on the top of each spinner allowed us to keep track of the center of mass positions of individual spinner versus time, measured rotation of the bar-code about the center of mass allowed us to know the spin angular momentum of each spinner as a function of time.

Single spinners where studied to determine the effective rate of flow of translational energy into a spinner due to air turbulence, the effective translational damping coefficient η, the applied torque $\tau_{drive} = 3.4 \times 10^{-5}$ N m of the mounted blowers and the the rotational damping coefficient $\eta_\varphi = 1.01 \times 10^{-6}$ N m s. The mass of each spinner was 0.025 kg, and the moment of inertia about the center of mass I_{cm} was determined by measuring the oscillation frequency ω for small angular displacements a known distance r from the center of mass (See Sec.II A for details). We determined I_{cm} to be 1.02×10^{-5} kg m^2.

II. DETERMINATION OF PHYSICAL PARAMETERS

A. Determination of the Spinner Moment of Inertia

We let the spinner of mass M oscillates around a fixed pivot axis in the horizontal plane (see Fig. S1A). The axis is located at distance equal to the inner radius (gear teeth excluded) R_{in} away from the center of the spinner. The moment of inertia of this physical pendulum I_{piv} is given by:

$$I_{piv} = \kappa_{piv} M R_{in}^2 \ , \ \kappa_{piv} = \left(\frac{T_{piv}^{(1)}}{2\pi} \right)^2 \frac{g}{R_{in}} - 1 \ , \tag{1}$$

where g is the gravitational acceleration and $T_{piv}^{(1)}$ is the time-period of the oscillation.

Direct measurements give $M = 0.025$kg and $R_{in} = 0.03$m. Using $g = 9.8\text{m/s}^2$, and from 5 measurements of 20-cycle time $T_{piv}^{(20)} = 20 T_{piv}^{(1)} = 8.6 \pm 0.2$s, we obtain $\kappa_{piv} = 0.52 \pm 0.07$. Note that the spinner radius (gear teeth included) is $R = 0.035$m, therefore:

$$I_{piv} = MR^2 \ \times \ (0.38 \pm 0.06) \quad \sim \quad MR^2 \ \times \ 1/3 \ . \tag{2}$$

Measurement using the trifilar pendulum method [1] also yields a similar result (see Fig. S1B).

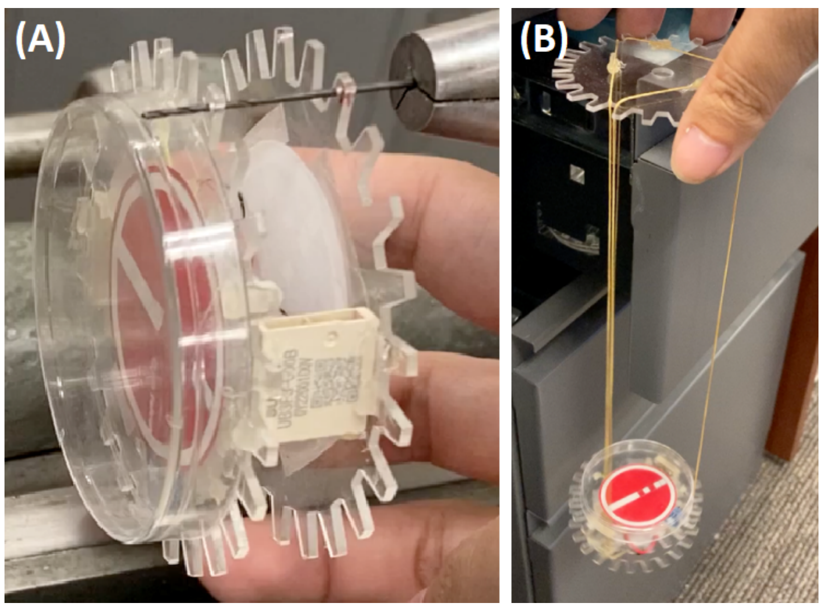

FIG. S1. (A) Pivot axis pendulum method. (B) Trifilar pendulum method.

B. Air-Flow and Drag

It should be noted the air table has a very non-trivial flow-profile, therefore it is worthwhile to obtain some statistics about it. We assume that the interaction between the air bed and a spinner at position $\vec{X}(t)$ results in a total force $\vec{F}$ which has a spatial-dependence average $\vec{f}(\vec{x})$, random fluctuation $\vec{\xi}(x,t)$ and a drag $-\eta_{trans}\vec{V}$:

$$M \frac{d^2}{dt^2} \vec{X}(t) = \vec{F}(t) = \vec{f}(\vec{x}) \Big|_{\vec{x}=\vec{X}(t)} + \vec{\xi}(x,t) - \eta_{trans} \vec{V}(t) \ , \ \vec{V}(t) = \frac{d}{dt} \vec{X}(t) \ . \tag{3}$$

From the trajectories of single spinners in the arena, we can estimate $\langle \vec{V} \rangle$, $\vec{f}/M$, $\sqrt{\langle \vec{\xi}^2 \rangle / M^2}$ and η_{trans}/M for any given position $\vec{x}$. The results does not seem to depend on whether the spinners are spin-up, spin-down or passive (blowers off), and are given in Fig. S2.

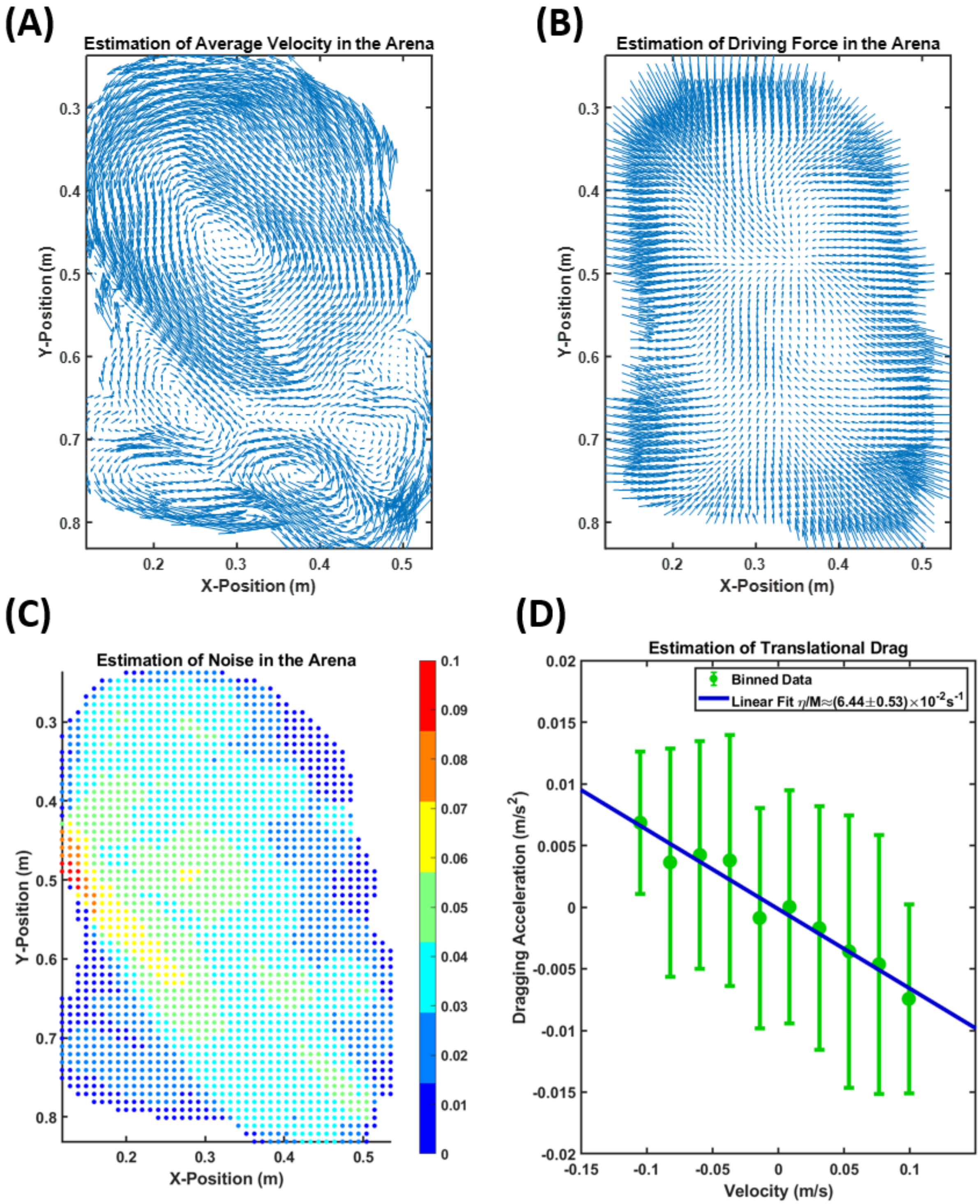

FIG. S2. (A) The vector-profile of the average spinner velocity $\langle\vec{V}\rangle$. (B) The vector-profile of the average air driving-force $\vec{f}/M$. (C) The average noise strength $\sqrt{\langle\vec{\xi}^2\rangle/M^2}$. (A) Estimation of the drag η_{trans}/M by looking at the relationship between the average spinner velocity and the dragging acceleration (which is just the acceleration but exclude the contribution from the driving-force).

III. SPINNER INTERACTION AND ITS COLLECTIVE EFFECT

A. Pairwise Interaction of Spinners

We need to understand the reciprocal interactions between the spinners. Consider a collision between two spinners (of radius R, mass M, and moment of inertial I) having angular velocities ω_1 and ω_2 in their center-of-mass frame so that they travel at the same velocity u but in opposite directions, with impact parameter b (see Fig. S3A). After the collision, the total impulse they each receive is $J_\parallel$ and $J_\perp$ in the parallel direction $\hat{\parallel}$ and the perpendicular direction $\hat{\perp}$ with respect to the tangent of their contact points, so that their velocities vector and angular velocities become $\vec{v}_1' = \left(v_{1\parallel}', v_{1\perp}'\right)$, $\vec{v}_2' = \left(v_{2\parallel}', v_{2\perp}'\right)$ and ω_1', ω_2' (see Fig. S3B). Thus, define $\theta = \arcsin(b/2R)$, we have:

$$u_{1\parallel} = -u_{2\parallel} = u\cos\theta\ ,\ u_{1\perp} = -u_{2\perp} = -u\sin\theta\ . \tag{4}$$

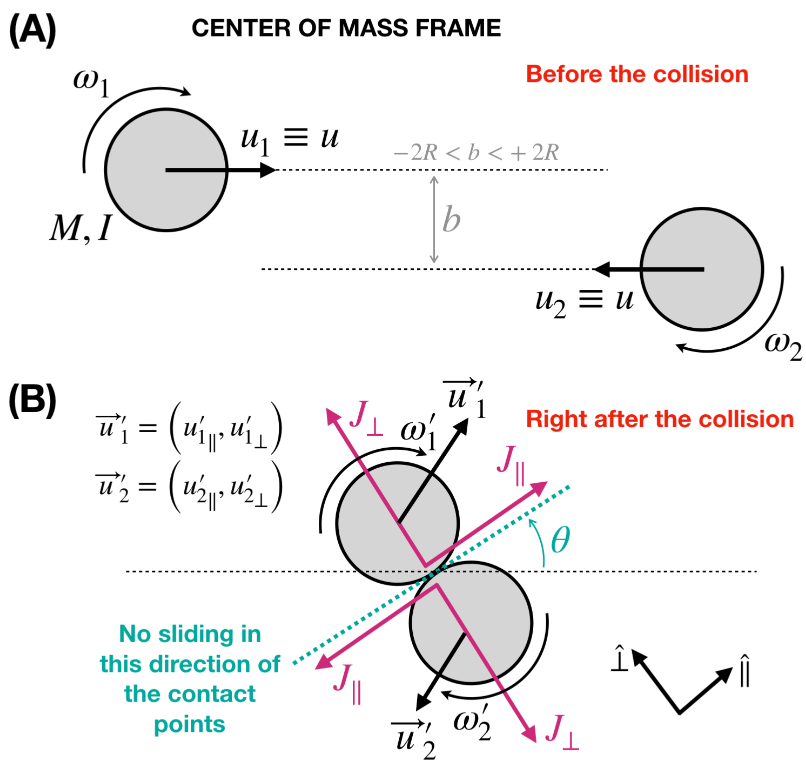

FIG. S3. In the center-of-mass frame of two spinners: (A) Before the collision. (B) Immediately after the collision.

The impulses relates the kinematic variables before and after the collision:

$$\begin{aligned} u_{1\parallel}' &= u_{1\parallel} + J_\parallel/M\ ,\ u_{2\parallel}' = u_{2\parallel} - J_\parallel/M\ ,\\ u_{1\perp}' &= u_{1\perp} - J_\perp/M\ ,\ u_{2\perp}' = u_{2\perp} + J_\perp/M\ ,\\ \omega_1' &= \omega_1 - J_\parallel R/I\ ,\ \omega_2' = \omega_2 - J_\parallel R/I\ . \end{aligned} \tag{5}$$

As a sanity check, by direct substitution of Eq. (5) one can show that the total angular momentum is conserved $L_{before} = L_{after}$ for all $\left(J_\parallel, J_\perp\right)$:

$$\begin{aligned} L_{before} &= I\omega_1 + I\omega_2 + M\left(\frac{b}{2}\right)u_1 - M\left(\frac{b}{2}\right)u_2 = I\omega_1 + I\omega_2 + MRu_{1\parallel} - MRu_{2\parallel}\ ,\\ L_{after} &= I\omega_1' + I\omega_2' + MRu_{1\parallel}' - MRu_{2\parallel}'\ . \end{aligned} \tag{6}$$

Since the spinners are gears with teeth, the no-sliding condition at their contact points in the $\hat{\parallel}$-direction is enforced right after the collision:

$$u_{1\parallel}' - R\omega_1' = u_{2\parallel}' + R\omega_2'\ . \tag{7}$$

Plug Eq. (4), Eq. (5) into Eq. (7), we can solve for $J_\parallel$:

$$\begin{aligned}\left(u\cos\theta + J_\parallel/M\right) - R\left(\omega_1 - J_\parallel R/I\right) &= \left(-u\cos\theta - J_\parallel/M\right) + R\left(\omega_2 - J_\parallel R/I\right)\\ \Rightarrow\ J_\parallel &= \frac{-2Mu\cos\theta + MR(\omega_1+\omega_2)}{2\left(1+MR^2/I\right)}\ ,\end{aligned} \tag{8}$$

and thus obtain the relation between angular velocities before and after the collision:

$$\begin{aligned}\omega_1' = \omega_1 - \frac{J_\parallel R}{I} = \omega_1 - \frac{MR^2}{2\left(I+MR^2\right)}\left(\omega_1+\omega_2\right) + \frac{2MRu\cos\theta}{2\left(I+MR^2\right)} &\xrightarrow[-2R<b<+2R]{\text{averaging over } b} \omega_1' - \omega_1 = -\frac{\omega_1+\omega_2}{2\left(1+I/MR^2\right)}\ ,\\ \omega_2' = \omega_2 - \frac{J_\parallel R}{I} = \omega_2 - \frac{MR^2}{2\left(I+MR^2\right)}\left(\omega_2+\omega_1\right) + \frac{2MRu\cos\theta}{2\left(I+MR^2\right)} &\xrightarrow[-2R<b<+2R]{\text{averaging over } b} \omega_2' - \omega_2 = -\frac{\omega_1+\omega_2}{2\left(1+I/MR^2\right)}\ ,\end{aligned} \tag{9}$$

Define the inertial parameter $\beta = 1/2(1+I/MR^2) < 1/2$, then after averaging over the impact parameter b we get the simplification:

$$\omega_1' - \omega_1 = \omega_2' - \omega_2 = -\beta\left(\omega_1+\omega_2\right)\ . \tag{10}$$

We will use this kinematic relationship to study the behavior of a many-spinner ensemble with two opposite-chirality (+ for counter-clockwise spinners and $-$ for clockwise spinners).

B. The Emergence of Collective Spin-Pumping

Consider $N = N_+ + N_-$ total number of spinners with N_+ counter-clockwise spinners and N_- clockwise spinners on an arena of area size A and perimeter length P, for each spinner the available area of the other $N-1$ spinners is about $(A-PR)-(2R)^2$ since their centers cannot get closer than $2R$. If the average velocity is $\langle v\rangle$ then during the time Δt a spinner can collide with any spinner inside a swept region of area $4R\langle v\rangle\Delta t$ (see Fig. S4).

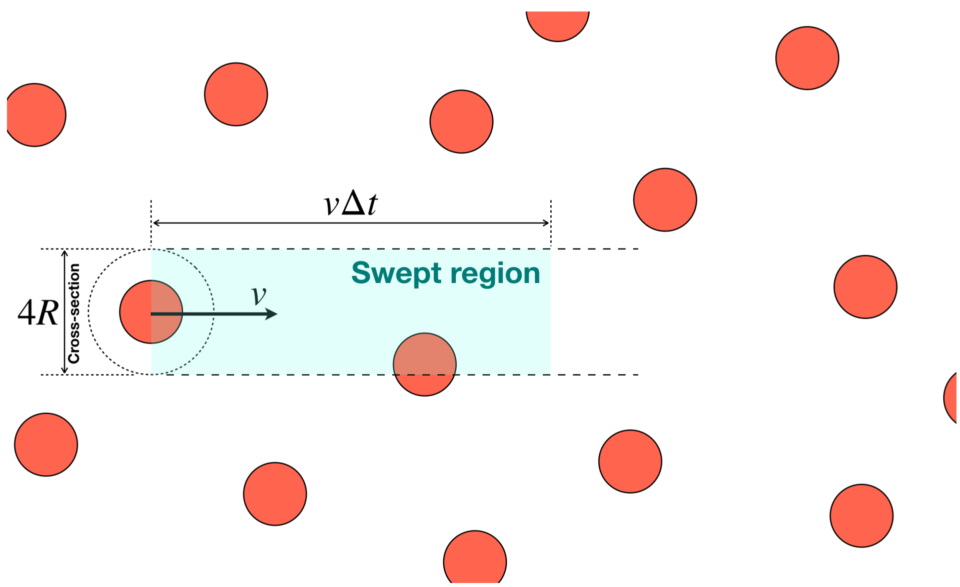

FIG. S4. During the time Δt, on average a spinner sweeps a region of area $4R\langle v\rangle\Delta t$.

The characteristic collision time τ can be estimated by associating the time scale $\Delta t = \tau$ for the expectation of encountering 1 other spinner in the swept region:

$$4R\langle v\rangle\Delta t\ \times\ \left.\frac{N-1}{(A-PR)-\pi(2R)^2}\right|_{\Delta t=\tau} \sim 1\ \ \Rightarrow\ \ \tau = \mathcal{O}(1)\ \times\ \left(\frac{A-PR-4\pi R^2}{4R\langle v\rangle}\right)\frac{1}{N-1}\ . \tag{11}$$

Due to relative translational motion between spinners, the coefficient $\mathcal{O}(1)$ is roughly $\sim 1/\sqrt{2}$ [2]. We can lump the pre-factor together into $\epsilon \sim (A-PR-4\pi R^2)/4R\langle v\rangle$, so that $\tau = \epsilon/(N-1)$. Note that, in general, for τ as a function of density, even for the simplest cases of a two-dimensional hard-disk gas, the dependency is complicated. We refer to the following paper [3] for a more thorough and numerical calculation.

Now let us make a mathematical estimation for the average value of the spinning velocity $\langle\omega_\pm\rangle$:

$$\frac{d}{dt}\langle\omega_\pm\rangle \approx \frac{N_\pm - 1}{N-1}\Big[-\frac{\beta\left(\langle\omega_\pm\rangle + \langle\omega_\pm\rangle\right)}{\tau}\Big] + \frac{N_\mp}{N-1}\Big[-\frac{\beta\left(\langle\omega_\pm\rangle + \langle\omega_\mp\rangle\right)}{\tau}\Big] \pm \frac{\int \Gamma_{\omega_\pm(t)} dt}{\tau}\Bigg|_{\langle\omega_\pm\rangle}, \tag{12}$$

where on the right side the first term represents the change due to a collision between spinners with the same chirality, the second term represents the change due to a collision between spinners with the opposite chirality, as followed from Eq. (10). The third term represents the average change of angular velocity between consecutive collisions. The angular acceleration $\pm\Gamma_{\omega_\pm}$ is a function of $\omega_\pm$, in general can be can be approximated by a Taylor's expansion as followed [4, 5]:

$$\pm\Gamma_{\omega_\pm} = \Gamma_\pm^{(0)} + \Gamma_\pm^{(1)}\omega_\pm + \mathcal{O}(\omega_\pm^2)\ . \tag{13}$$

Physically, we can assume that the air-blowers generate a constant torque contribution and there is a drag effect which is proportional to the spinning speed. Match with the description in Eq. (13), $\Gamma_\pm^{(0)} = \pm\gamma$ is set by that torque and $\Gamma_\pm^{(0)} = -\eta_{rot}$ is set by that drag. Define $\Omega = \gamma/\eta_{rot}$, we get:

$$\pm\Gamma_{\omega_\pm} = \pm\gamma - \eta_{rot}\omega_\pm = \pm\gamma\left(1 \mp \frac{\omega_\pm}{\Omega}\right)\ , \tag{14}$$

in which Ω is the maximum possible angular-velocity of a single isolated spinners plays a similar role to that of the carrying capacity in growth dynamics [6]. This model turns out to be in great agreement with how a single isolated aerial spinner accelerates its rotational motion (see Fig. S5).

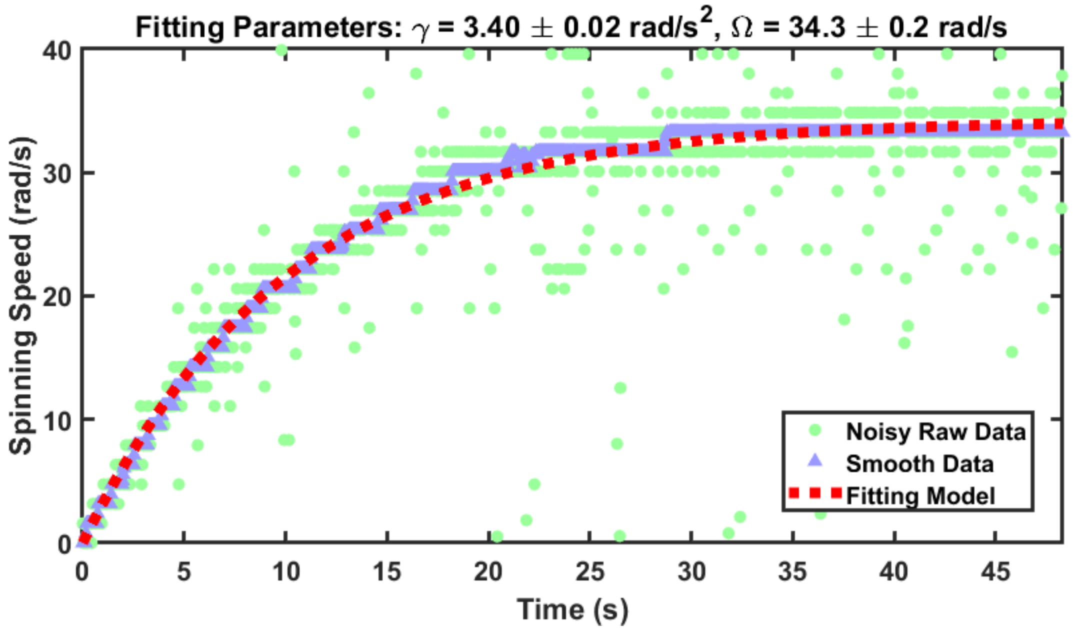

FIG. S5. We investigate how a single isolated spinner floating on the air-bed accelerate its spinning speed. Here we fit the model described by Eq. (14) with the data (the raw data was obtained at framerate 30 fps, the smooth data comes from moving median inside a 2-seconds window). The best-fit captures the observation nicely.

This linearity in Γ_ω simplifies Eq. (12):

$$\begin{aligned}
&\frac{\int \Gamma_{\omega_\pm(t)} dt}{\tau} = \frac{\int \gamma\left(1 \mp \omega_\pm(t)/\Omega\right) dt}{\tau} = \gamma\left[1 \mp \frac{\int \omega_\pm(t) dt/\tau}{\Omega}\right] = \gamma\left(1 \mp \frac{\langle\omega_\pm\rangle}{\Omega}\right) = \Gamma_{\langle\omega_\pm\rangle} \\
\Rightarrow\ &\frac{d}{dt}\langle\omega_\pm\rangle \approx \frac{N_\pm - 1}{N-1}\Big[-\frac{\beta\left(\langle\omega_\pm\rangle + \langle\omega_\pm\rangle\right)}{\tau}\Big] + \frac{N_\mp}{N-1}\Big[-\frac{\beta\left(\langle\omega_\pm\rangle + \langle\omega_\mp\rangle\right)}{\tau}\Big] \pm \Gamma_{\langle\omega_\pm\rangle}\ .
\end{aligned} \tag{15}$$

At the steady state, $d\langle\omega_\pm\rangle/dt = 0$, therefore we can solve Eq. (15) which is now just an algebraic equation to get:

$$\langle\omega_\pm\rangle = \pm\Omega \;\times\; \frac{\alpha\,(\alpha + 3N - 2 - 2N_\pm)}{(\alpha + 2N - 2)(\alpha + N - 2)}\,, \tag{16}$$

where $\alpha = \gamma\epsilon/\beta\Omega$ depends on the spinner translational locomotion and inertial properties, and the air-blowing strength. Use $\gamma \sim 3\text{rad/s}^2$ and $\Omega \sim 30\text{rad/s}$ as we find from Fig. S5, $\beta \sim 3/8$ (from the spinner inertial measured in Section I) and $\epsilon \sim 25\text{s}$ (we get this from the average translational velocity $\langle v\rangle \sim 7\text{cm/s}$, the spinner radius $R = 3.5\text{cm}$, the arena has area size $A \sim 55\text{cm}\times 75\text{cm}$ and perimeter length $P \sim 2(55 + 75) = 260\text{cm}$, and $\mathcal{O}(1) \sim 1/\sqrt{2}$), we can make an estimation that $\alpha \sim 7$.

Note that Eq. (16) applicable only with $N > 1$ and for $\langle\omega_\pm\rangle$ when $N_\pm > 0$. When $N_+ = 1$ and $N_- = 1$ we have $\langle\omega_\pm\rangle = \pm\Omega$, and for a fixed value of N then $\langle\omega_\pm\rangle$ monotonically decreases as $N_\pm$ increases: the minority will always spin faster than the majority! This finding is presented in Fig. S6. When there is only one spinner we have $|\langle\omega\rangle| = \Omega$. For a pure population of, without loss of generality, $N_+ = N > 1$ counter-clockwise spinners, then the average angular velocity at the steady state is:

$$\langle\omega_+\rangle = +\Omega \;\times\; \frac{\alpha}{\alpha + 2N - 2}\,. \tag{17}$$

This means the more spinners the slower they can spin on average.

In the limit $N \to \infty$, define $n_+ = N_+/N$ to be a fraction of counter-clockwise spinners, Eq. (16) simplifies:

$$\langle\omega_\pm\rangle = \pm\Omega \;\times\; \frac{\alpha\,(3 - 2n_+)}{2N}\,. \tag{18}$$

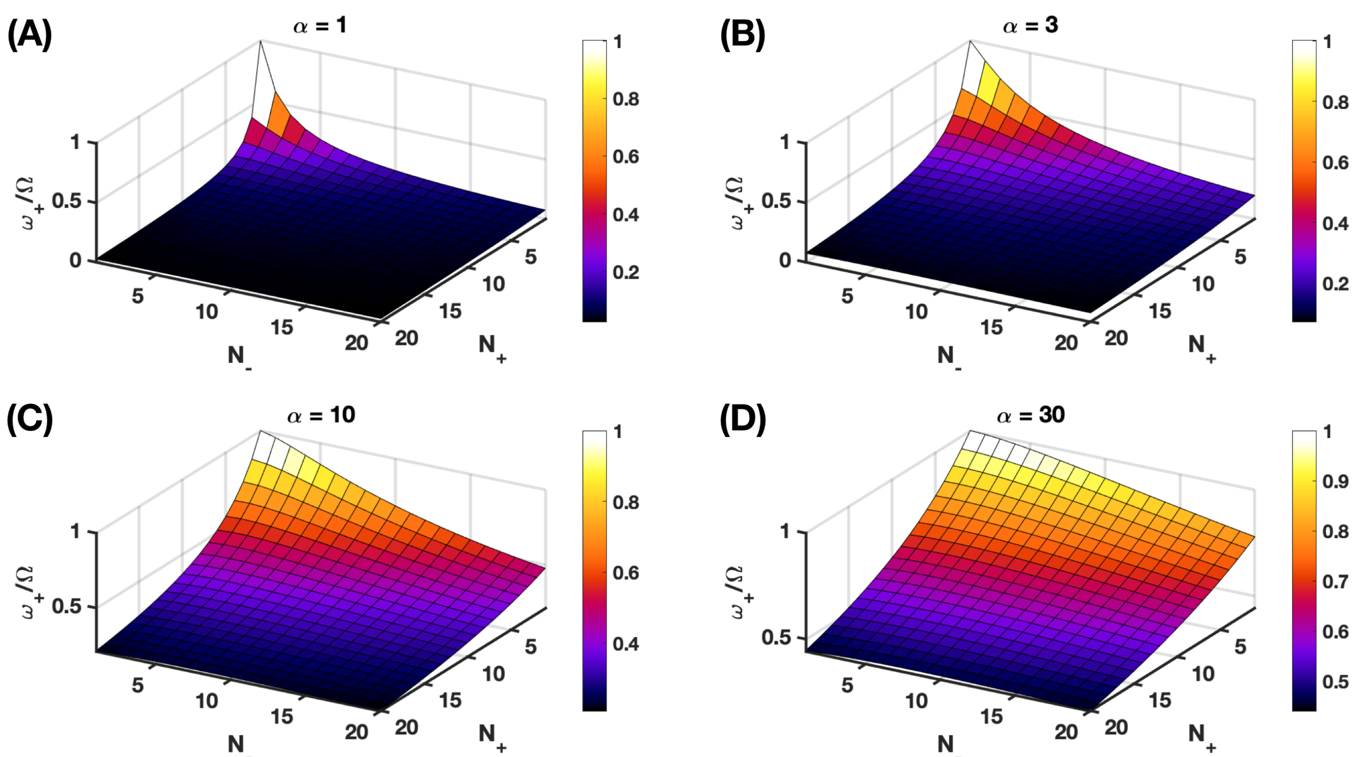

FIG. S6. The average spinning velocity $\langle\omega_+\rangle$ in the unit of Ω as a function of N_+ and N_- using Eq. (16), for different values of the parameter α: (A) $\alpha = 1$. (B) $\alpha = 3$. (C) $\alpha = 10$. (D) $\alpha = 30$.

IV. AVERAGE ROTATIONAL AND TRANSLATIONAL ENERGY OF SPINNERS

A. Rotational Energy

We can also make another crude estimation, for the average rotational energy E_{rot} of all spinners, using Eq. (16) and take the average rotational energy of each species ($\pm$) of spinners to be $E_{\pm,rot} = I\langle\omega_\pm\rangle^2/2$:

$$\begin{aligned} E_{rot} = \frac{N_+E_{+,rot} + N_-E_{-,rot}}{N} &= \frac{1}{2}I\Omega^2 \times \frac{\alpha^2\left[N_+\left(\alpha+3N-2-2N_+\right)^2 + N_-\left(\alpha+3N-2-2N_-\right)^2\right]}{N(\alpha+2N-2)^2(\alpha+N-2)^2} \\ &= \frac{1}{2}I\Omega^2 \times \frac{\alpha^2\left[N(\alpha+N-2)^2 + 4N(2\alpha+3N-4)N_+ - 4(2\alpha+3N-4)N_+^2\right]}{N(\alpha+2N-2)^2(\alpha+N-2)^2} \\ &= \frac{1}{2}I\Omega^2 \times \frac{\alpha^2\left[N(\alpha+N-2)^2 + (2\alpha+3N-4)N^2 - 4(2\alpha+3N-4)(N/2-N_+)^2\right]}{N(\alpha+2N-2)^2(\alpha+N-2)^2}\ . \end{aligned} \tag{19}$$

Here we expand E_{rot} as a sum series of N_+ (without loss of generality) and group then in a way that symmetry around $N/2$ (due to the interchangeable $N_+ \leftrightarrow N_-$). As a function of N_+ for a fixed value of N, we find that E_{rot} is an inverted parabola centered at $N_+ = N/2$. This is consistent with what we have found in Fig. 2B of the main manuscript. In the limit $N \to \infty$, Eq. (19) simplifies:

$$E_{rot} = \frac{1}{2}I\Omega^2 \times \frac{\alpha^2\left[1-3\left(1/2-n_+\right)^2\right]}{N^2}\ . \tag{20}$$

Up to a positive-constant energy shift, the form of Eq. (19) captures our observation quite nicely (see Fig. S7A).

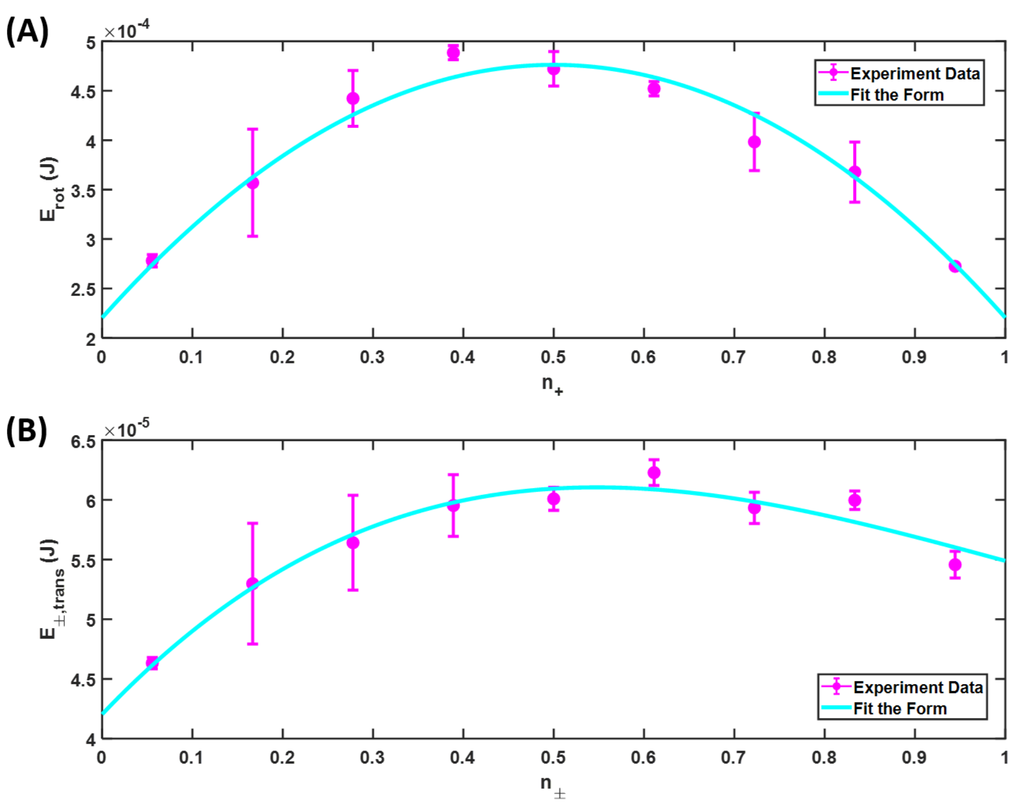

FIG. S7. (A) Rotational energy E_{rot} as a function of the fraction n_+ of the spinner species, fitting with the form Eq. (19) up to a positive-constant. (B) Translational energy $E_{\pm,trans}$ as a function of the fraction $n_\pm$ of the spinner species, fitting with the form Eq. (21) up to a positive-constant.

B. Translational Energy

We will use some qualitative argument to explain why maximum translational energy $E_{\pm,trans}$ of each species are somewhere between $n_\pm \in [1/2, 1]$ as shown in Fig. 2B of the main manuscript. In this system, the incoming energy is mostly from the blowers that make the spinners rotate and the air flows that drive the spinners moving. Also collisions between spinners of the same species turn rotational energy into translational energy. Thus the higher the rotation energy $E_{\pm,rot}$ and the more collisions between spinners of the same species $\propto n_\pm$, the bigger the translational energy $E_{\pm,trans}$ can be. Utilize the simplification Eq. (18), we obtain:

$$E_{\pm,trans} \propto (E_{rot} + E_{air})\, n_\pm \propto \left[(3-2n_\pm)^2 + \mathcal{E}_{air}\right] n_\pm \ , \tag{21}$$

where $\mathcal{E}_{air} > 0$ are is the possible contributions from the air flows. The maximum of this function in the range of $n_\pm \in [0, 1]$ should be inside $n_\pm \in [0, 1]$ for $\mathcal{E}_{air} \leq 3$:

$$n_\pm\Big|_{\max(E_{\pm,trans})} = 1 - \frac{1}{2}\sqrt{1 - \frac{\mathcal{E}_{air}}{3}} \ , \tag{22}$$

and right at the upper-limit value $n_\pm = 1$ for $\mathcal{E}_{air} > 3$. Up to a positive-constant energy shift, the form of Eq. (21) captures our observation quite nicely (see Fig. S7B).

V. THE DAMPED OSCILLATIONS OF MIXING ENTROPY

From the experiments, we can see that at a high enough population of spinners, a topological current can emerge on the outer-most layer while a jammed inner core can be formed. Consider $N = 36$, we observe that for $N_+ : N_- = 36 : 0$ the edge current circulates counter-clockwise, for $N_+ : N_- = 0 : 36$ the edge current circulates clockwise, and for $N_+ : N_- = 18 : 18$ there is no clear sign for an edge current (see Fig. S8). At lower-density, there is no edge current and the inner core is not jammed. While the following uses a graphic guidance where there is a clear distinction between a rotating outer layer and static inner core, in real situation where such distinction is more ambiguous, the inner core generalizes to an idle portion of spinner and the outer flow generalizes to the circulating spinners. We posit this simplified model still qualitatively captures the phenomenon.

Here we show how mixing entropy can oscillate due the emergent of a topological edge current at high-density of single species spiners. Say, in the beginning $t = 0$ (see Fig. S9A), the upper-half and the lower-half of the arena has equal number of spinners $N/2$. There are $O^u_u(0) = O^d_d(0) = \nu N/2$ in the upper-half and lower-half of the edge layer (which corresponds to the fast circulating boundary flow) and $I^u_u(0) = I^d_d(0) = (1-\nu)N/2$ in the upper-half and lower-half of the inner core, where $\nu < 1$ represents the fraction of the spinners on the edge layer. The low-density limit corresponds to $\nu \to 0$.

First, let's consider the edge layer does not circulate around the inner core. To describe the mixing phenomenon, we will assume the following simple dependency:

$$\begin{gathered}\tilde{O}^u_u(t) = O^u_u(0)\left(\frac{1+e^{-t/T_O}}{2}\right) \ , \ \tilde{O}^d_d(t) = O^d_d(0)\left(\frac{1+e^{-t/T_O}}{2}\right) \ , \\ \tilde{O}^d_u(t) = O^u_u(0) - \tilde{O}^u_u(t) \ , \ \tilde{O}^u_d(t) = O^d_d(0) - \tilde{O}^d_d(t) \ ,\end{gathered} \tag{23}$$

and:

$$\begin{gathered}\tilde{I}^u_u(t) = I^u_u(0)\left(\frac{1+e^{-t/T_I}}{2}\right) \ , \ \tilde{I}^d_d(t) = I^d_d(0)\left(\frac{1+e^{-t/T_I}}{2}\right) \ , \\ \tilde{I}^d_u(t) = I^u_u(0) - \tilde{I}^u_u(t) \ , \ \tilde{I}^u_d(t) = I^d_d(0) - \tilde{I}^d_d(t) \ .\end{gathered} \tag{24}$$

These equations only have mixing in the edge layer only and the inner core only but no exchange of spinners between these. Of course reality, there should also be mixing between the edge layer and the inner core too, but the results that we see with our simplification will not be different (and the advantage is that the math becomes much more tractable).

For the edge layer circulates around the inner core with angular velocity Ω (see Fig. S9B), we have:

$$\begin{aligned}O^u_u(t) &= \tilde{O}^u_u(t)\Delta\left(\frac{\pi - \Omega t}{2\pi}\right) + \tilde{O}^d_u(t)\Delta\left(\frac{\Omega t}{2\pi}\right) \ , \\ O^d_d(t) &= \tilde{O}^d_d(t)\Delta\left(\frac{\pi - \Omega t}{2\pi}\right) + \tilde{O}^u_d(t)\Delta\left(\frac{\Omega t}{2\pi}\right) \ ,\end{aligned} \tag{25}$$

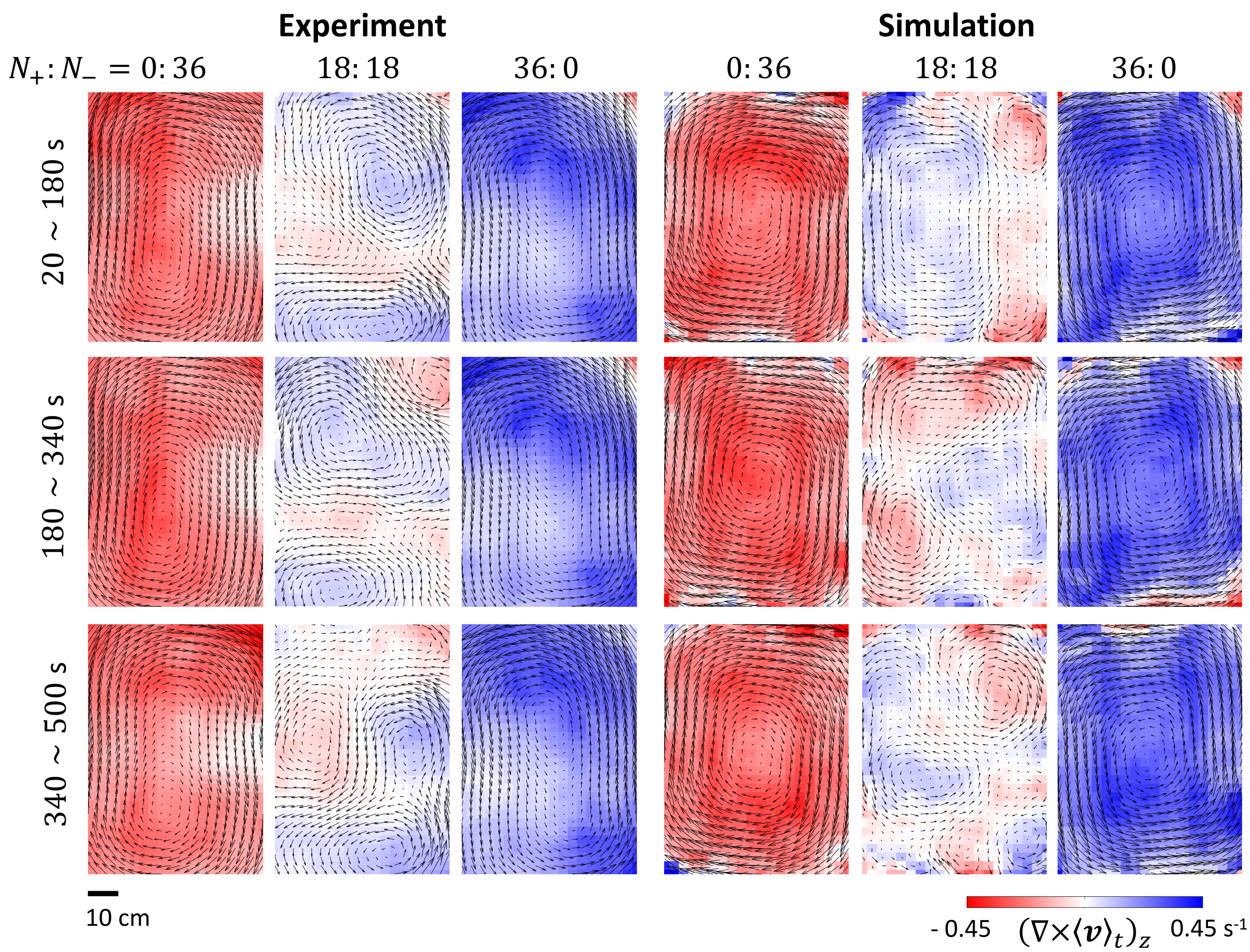

FIG. S8. The evolution of the time-window-averaged velocity profile for 36-spinner collectives in which $N_+ : N_-$ are 36 : 0, 18 : 18 and 0 : 36. The color shows the vorticity ($\zeta = (\nabla \times \langle \mathbf{v} \rangle)_z$). From the time evolution, we can see there are multiple vortices in the even-mixture case and the vortices are motile in both simulation and experiment. To count the number of vortices (Fig.3F in the main text), we use the bwconncomp function in MATLAB to find the number of connected components for $\zeta > 0$ and $\zeta < 0$. Vortices larger than 3% of the arena sizes are considered.

and:

$$I_u^u(t) = \tilde{I}_u^u(t) \ , \ I_d^d(t) = \tilde{I}_d^d(t) \ , \tag{26}$$

in which we use the triangle-wave function:

$$\Delta(\xi) = 2\left|\xi - \left\lfloor \xi + \frac{1}{2} \right\rfloor\right| . \tag{27}$$

The joint probabilities are given by:

$$p_u^u = \frac{O_u^u(t) + I_u^u(t)}{O_u^u(0) + I_u^u(0)} \ , \ p_d^d = \frac{O_d^d(t) + I_d^d(t)}{O_d^d(0) + I_d^d(0)} \ , \tag{28}$$

and the mixing entropy can be calculated as:

$$\begin{aligned} S(t) &= -p_u^u \ln p_u^u - p_u^d \ln p_u^d - p_d^d \ln p_d^d - p_d^u \ln p_d^u \\ &= -p_u^u \ln p_u^u - (1 - p_u^u) \ln (1 - p_u^u) - p_d^d \ln p_d^d - \left(1 - p_d^d\right) \ln \left(1 - p_d^d\right) \ . \end{aligned} \tag{29}$$

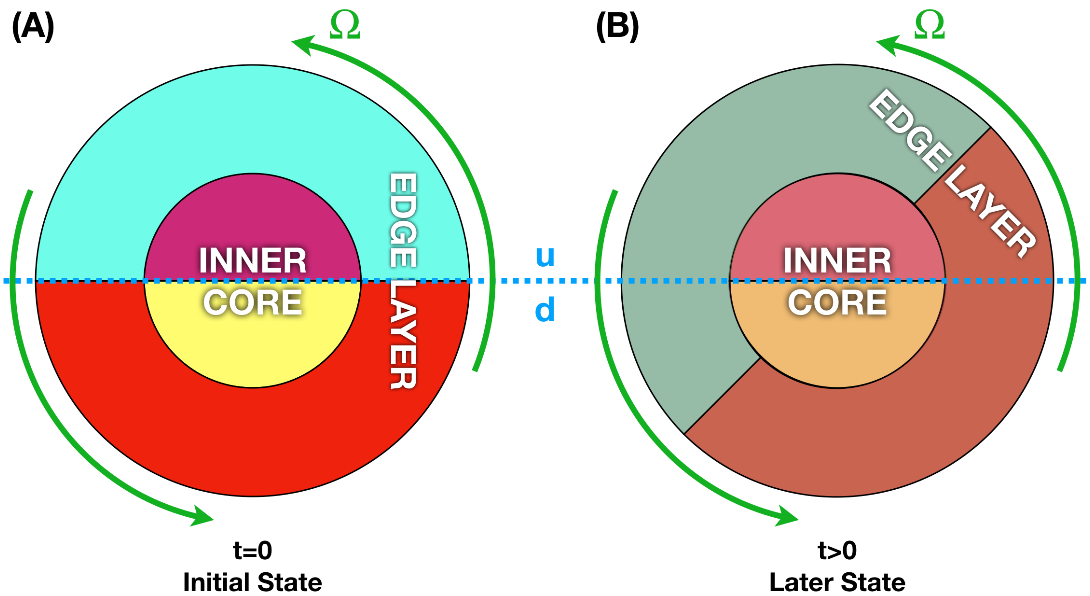

FIG. S9. The emergent of a topological edge current can explain what is going on with mixing entropy and how recurrences can happen.

We can plot $S(t)$ depends on the parameters (Ω, T_O, T_I) as shown in Fig. S10. While the function is not as smooth as seen in our experiments, this model still qualitatively captures the damping oscillation nonetheless. Moreover, if we change $\Delta(\cdot)$ to $\sin(\cdot)$, the evolution will become smoother and closer to the data in experiments due to the smear-out of the rotating spinner strip.

The recurrence time T_{recc} is equal to half of the circulation time $T_{circ} = 2\pi/\Omega$. From the experiments we see $T_{circ} \sim 60$s, therefore we can estimate $T_{recc} \sim 30$s. This finding is indeed in agreement with the mixing entropy oscillation!

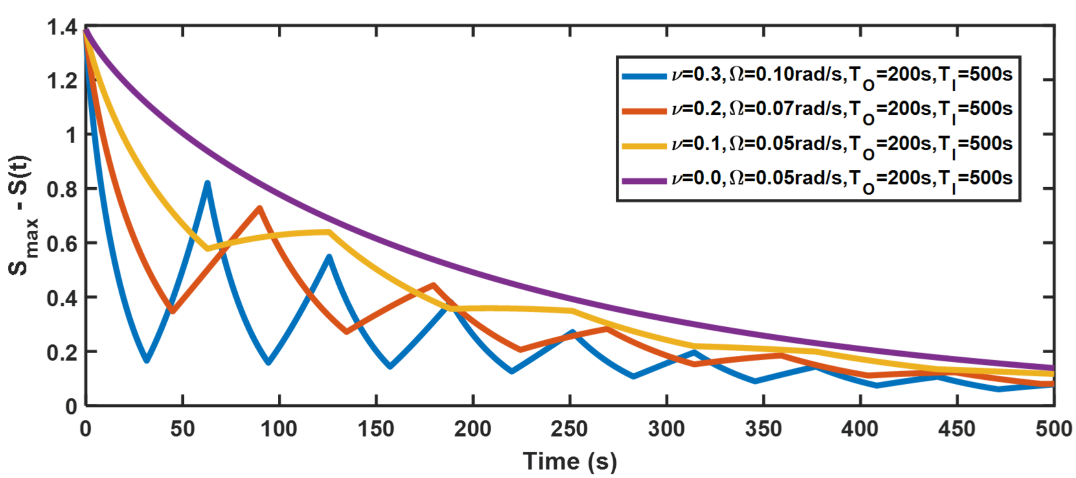

FIG. S10. The mixing entropy $S(t)$ as given in Eq. (29) exhibits a damped oscillating behavior.

VI. GEARS MADE OF GEARS

Gears are toothed, mechanical transmission elements used to transfer motion and power between components of machines. They are ubiquitous, can be found within a large range of length-scales. Since the designing and operation principles of gears are independence of size, it is very convenient to use them for creating scale-free fractal structures in which low-level small gears drive higher-level big gears. We can use our spinners as the fundamental gears, put some of them inside a ring with teeth to get a structure which can also works like a gear (see Fig. S11A). Repeating this we can build Matryoshka superstructures of scale-free fractal gears (see Fig. S11B).

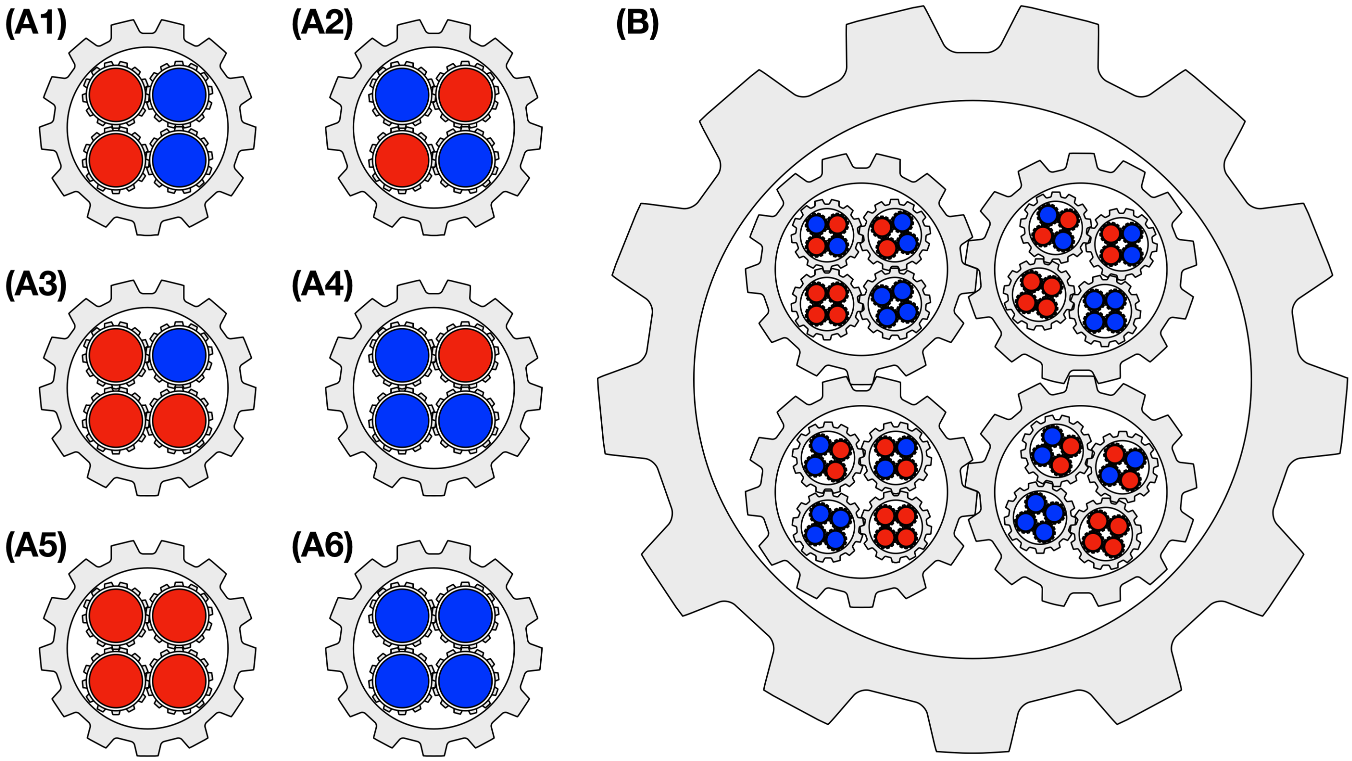

FIG. S11. (A1-6) Some examples of gears made of fundamental gears, which are spinners. Here we list all possible topological arrangement with four fundamental gears, and (A1-2) are the designs we investigate in the main manuscript. (B) A scale-free fractal gear, which is three-level above the fundamental gears, larger in size but same designing and operation principles.

For 4 spinners geometrically confined by an outer gear which is a toothed ring as described in the main manuscripts, there are 6 possible arrangements (see Fig. S11A1-6) with spaces in between gears. It should be noted that, for simple design, the ring only has outer-teeth but no inner-teeth, which means the inside gears powered the outside gears via frictional couplings.

There are many possible configurations for the positions of spinners and for the locking-interaction between them. This degeneracy gives rise to spinning frustration – there exists no steady state of spinning as these gears made of gears keeps jumping between different configurations which can be seen from the intermittency of their rotational motion. We call them the frustrated spinning states. We show that each frustrated spinning state corresponds to a rotational mode, with distinct average angular velocity $\langle\dot{\Theta}\rangle$ and rotational energy as shown in Fig. S12. The more homogeneous (single-species) the faster they can spin, and for equal number of spin-up and spin-down they pretty much cannot spin (due to symmetry cancelling out torque contributions).

The special cases $N_+ : N_- = 2 : 2$, which is considered in the main manuscripts, has two possible topological arrangements (parallel or diagonal same-species). Even though they both does not spin very much on average, the average and intermittency of rotational energies are not the same.

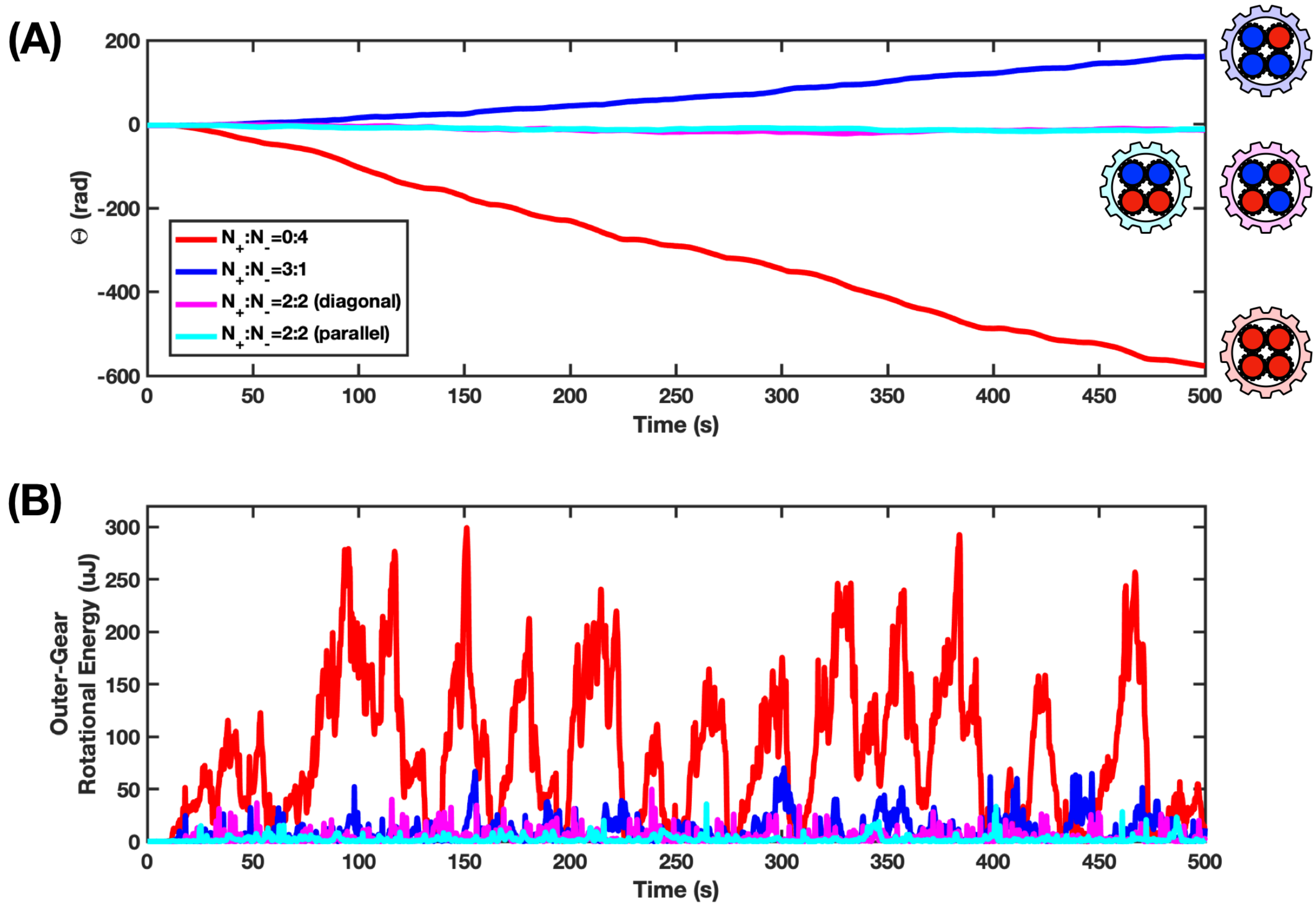

FIG. S12. (A) The rotation of the outer-gear, angle Θ is positive if it is turned counter-clockwise. (B) The rotational energy of the outer-gear, which exhibits an intermittency behavior for all arrangements of 4 spinners inside.

VII. SIMULATION

A. Model

In the simulation, each spinner is subjected to the collision force from another spinner $\mathbf{F}_{coll}$, translational drag force $\mathbf{F}^{trans}_{drag}$, rotational driving torque τ_{drive} from the blowers on spinner, rotational drag torque τ^{rot}_{drag}, air current flow $\mathbf{F}_{air}$, and collision force from the boundary $\mathbf{F}_{wall}$ (Fig.S13A,B). The parameters are determined from direct and indirect physical measurement as listed in the following table.

	Description	Value	Reference
m	Spinner mass	0.025 kg	Direct measurement from a scale
R_0	Spinner outer radius	0.035 m	Direct measurement from a caliper
R_i	Spinner inner radius	0.030 m	Same as above
I	Spinner moment of inertia	1.01×10^{-5} kg m^2	Sec.II A of this document
Ω	Saturated angular velocity of the orbit	32 rad s^{-1}	Fig.S5
γ	Rotational driving acceleration	3.4 rad s^{-2}	Same as above
τ_{drive}	Rotational driving torque	3.4×10^{-5} N m	$= I\gamma$
η	Translational drag coefficient	1.6×10^{-3} kg s^{-1}	$= m \cdot 6.5 \times 10^{-2}$ s^{-1}. See Fig.S2D.
η_φ	Rotational drag coefficient	1.06×10^{-6} N m s	$= \tau_{drive}/\Omega$
F_{air}	Air current force		See the cubic fit in Fig.S13A inset.
A_1	Half arena length	0.38 m	Direct measurement from a meter stick
A_2	Half arena width	0.28 m	Same as above

TABLE S1. **List of parameters used in physical simulations.**

For the spinner-spinner collision force, Each spinner is modeled as line segments connected to each other and uses the exact geometry of the spinner. The spinner-spinner interaction is evaluated as the sum of all pairwise interactions between the line segments of the two spinners. The line-line interaction uses spring-dash model, which regards the strain as the virtual overlap of the two line segments $F_{coll} = k_s\delta + k_d\delta v_n$ where v_n is the relative velocity projected in the normal direction (Fig.S13C). k_s and k_d are phenomenological parameters such that the coefficient of restitution and the collision pattern $\Delta\omega = -\beta(\omega_1 + \omega_2)$ matches with the experiment (Fig.S14A). In simulations, we use $k_s = 10^4$ N/m,$k_d = 2 \times 10^5$ N s/m^2.

B. Numerical method

The code was first developed in MATLAB for visual convenience and then manually compiled into C++ for efficiency. The numerical scheme uses an sympletic integrator, velocity-Verlet [**?**] to reduce accumulated numerical errors. The time step uses 10^{-4} second considering the largest Jacobian related to the collision is $\sim 10^4$ second^{-1} as we choose the collision elasticity to be 10^4 N/m. The elasticity is phenomenonlogical and yet physically realistic that the collision result is insensitive to the elasticity value given the order of magnitude is $\sim 10^4$ N/m.

As a test, we evaluate a simulation at equilibrium condition (without air current force, rotational or translation drag or drive) where 18 non-active spinners started with pure translational motion. Over time, a portion of translational energy gradually converts to rotational energy and eventually shows equipartition in rotational (1 degree of freedom) and translational energy (2 degrees of freedom), i.e. $\frac{1}{2}m\langle v_i^2\rangle_i/2 = \frac{1}{2}I\langle\omega_i^2\rangle_i/1$ [**?**]. It is an interesting feature that with concave geometry, there can be tangential interaction without having dissipative forces [**?**].

C. Results

We first simulate the collective behavior of the 18-spinner and 36-spinner systems. All simulation runs for 500 s to be consistent with the experiments. See SI5.mp4 for the simulation. For each spin ratio, an ensemble of 10 simulations is done to evaluate the kinetic energies' and mixing time's dependence on spin ratio. Without fine tuning, the results match with experiments except for small quantitative deviation. Further, the small vortices for regimes without global circulation also show motile vortices as we observe in experiments (Fig.S8). We further use simulations explore cases with $N = 24, 30$ to search for the boundary between the regimes with and without global circulation (Fig.3E,F in the main text).

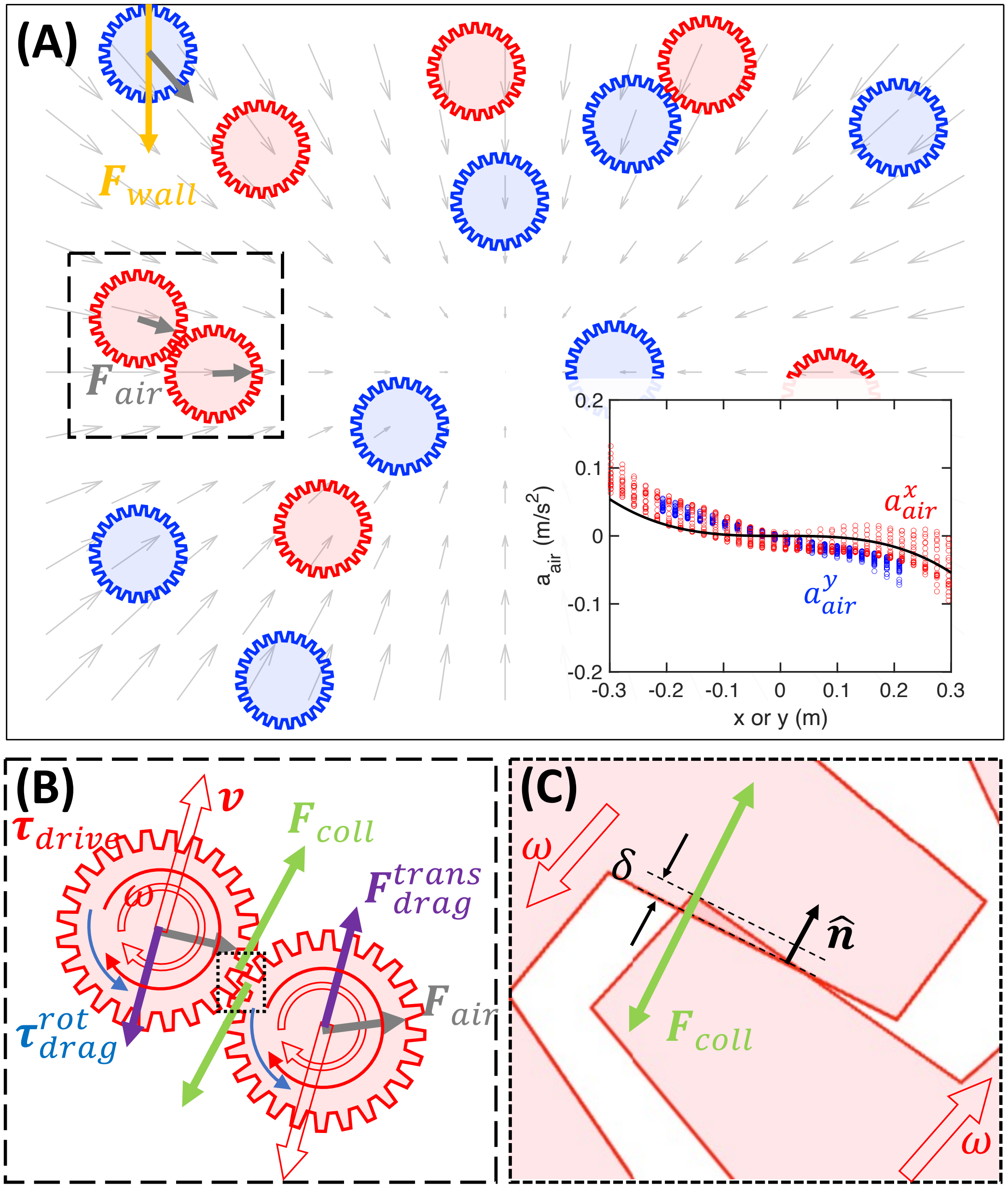

FIG. S13. **Simulation setup.** (A) Each spinner is subjected to the air current force $\mathbf{F}_{air}$ and the normal force from the boundary $\mathbf{F}_{wall}$. Inset: the components of $\mathbf{a}_{air} = \mathbf{F}_{air}/m$. The black cubic fit shows the air current force used in simulation. (B) Besides the collision force $\mathbf{F}_{coll}$ from another spinner, each spinner is also subjected to a translational drag force $\mathbf{F}^{trans}_{drag}$, which is antiparallel to the velocity $\mathbf{v}$. In the rotational direction, each spinner is subjected to a driving torque τ_{drive} from the blowers on the spinner and a rotational drag torque τ^{rot}_{drag}. (C) In simulation, the collision force uses a spring-dash model where the collision force is composed of a restoring force proportional to the virtual overlap δ and a dissipation dash force proportional to both δ and the approaching velocity's projection in the normal direction $\hat{\mathbf{n}}$.

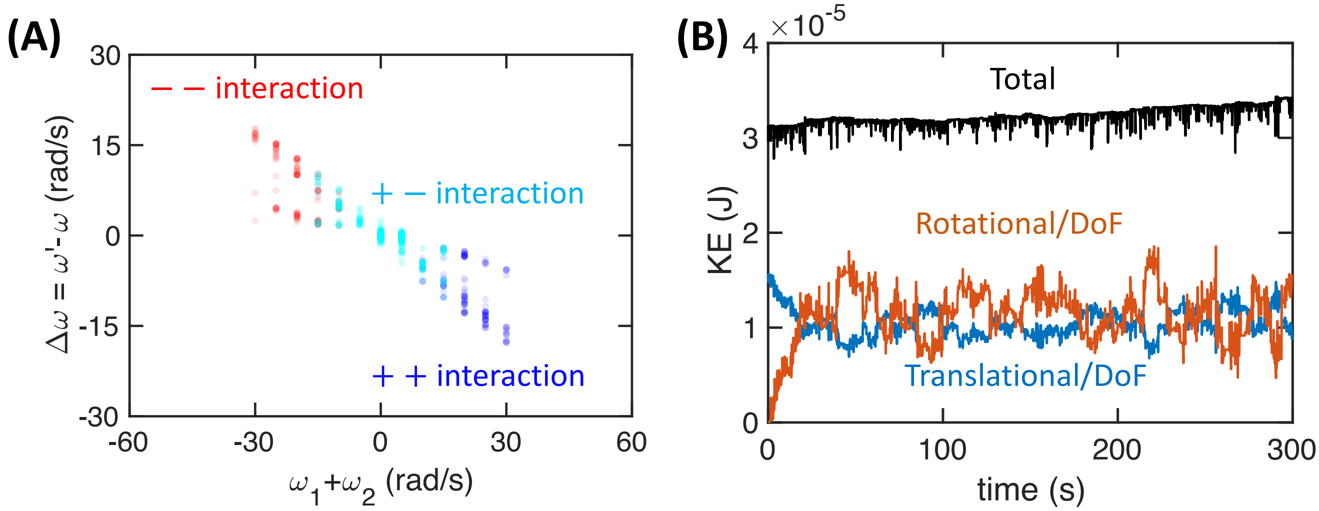

FIG. S14. **Simulation test.** (A) Change of angular velocity from simulation shows a negative proportionality with a slope -0.5, slightly larger than the -0.38 in experiment. (B) Without dissipation or injection of energy, 18 spinners started with pure translational energy converts part of the translational energy into rotational energy and shows equipartition. The value shown in this panel shows the energy per spinner per degree of freedom. The slight increase of total energy is from accumulative numerical error, which can improve with finer time steps. See SI5.mp4 for video.

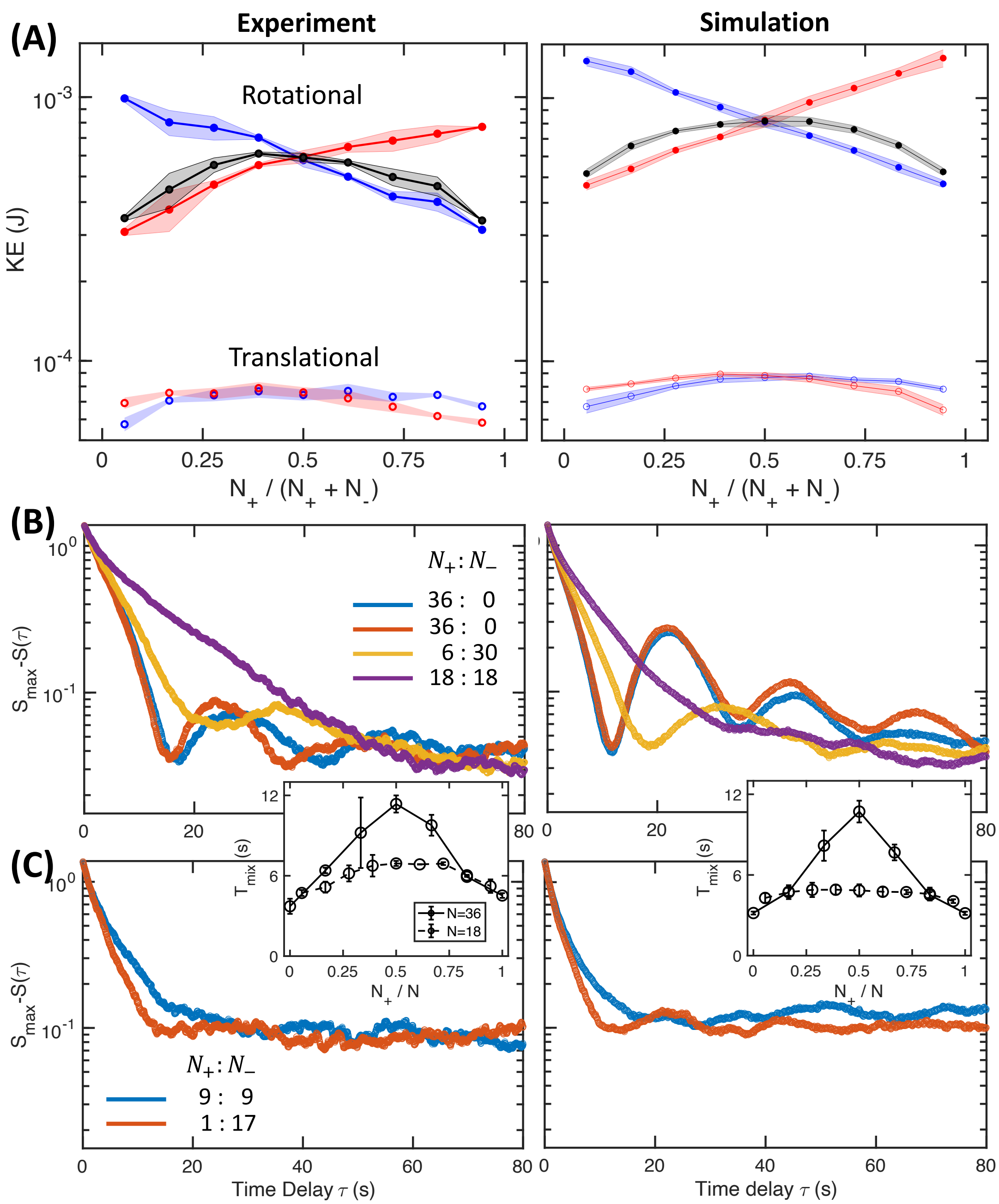

FIG. S15. **Simulation result.** Comparison of experiment and simulation in terms of (A) kinetic energies' dependence on spin ratio, (B) the mixing dynamics of a 36−spinner system, and (C) the mixing dynamics of a 18−spinner system.

VIII. SUPPLEMENTARY MOVIES

[SI1] Introduction to the spinners
This movie first introduces an individual spinner part by part, then shows the individual motion and collective motion from a perspective view, and finally shows two typical pairwise interactions, being the same-spin, and opposite-spin interactions.

[SI2] Collective motion of the spinners
This movie shows the collective motion with different spin-ratios ($N_+ : N_- = 0 : 1$, $0.5 : 0.5$, and $1 : 0$) at different number densities ($N = N_+ + N_- = 18$ and 36). The motion is displayed at both real time and three times faster.

[SI3] Mixing of marked spinners
This movie first visually demonstrates the method we use to obverse the mixing process, which leads to the evaluation of entropy change shown in the manuscript. The movie then shows the collective motion with different spin-ratios ($N_+ : N_- = 0 : 1$, $0.5 : 0.5$, and $1 : 0$) at different number densities ($N = N_+ + N_- = 18$ and 36). The spinners are also marked as in the method demonstration and the videos are displayed at both real time and three times faster.

[SI4] Fractal spinner
This movie shows the motion of two typical configurations composed of four spinners (two up spinners and two down spinners) in a confining ring (Fig. 4 in the main text).

[SI5] Simulation
This movie first shows the closeup of simulation at a speed 10 times slower than the real time. The movie then shows the collective motion reproducing the experiments shown in SI2. Finally, the movie shows the equipartition of energy holds in a simulation where all energy injection and dissipation are turned off.

[1] C. Schedlinski and M. Link, Mechanical systems and signal processing **15**, 189 (2001).
[2] M. Kardar, *Statistical physics of particles* (Cambridge University Press, 2007).
[3] A. Taloni, Y. Meroz, and A. Huerta, Physical Review E **92**, 022131 (2015).
[4] B. Taylor, *Methodus incrementorum directa et inversa* (Innys, 1717).
[5] G. B. Thomas, *Calculus and analytic geometry* (Addison-Wesley, 1968).
[6] T. V. Phan, G. Wang, T. K. Do, I. G. Kevrekidis, S. Amend, E. Hammarlund, K. Pienta, J. Brown, L. Liu, and R. H. Austin, Journal of Biological Physics **47**, 387 (2021).